HHS Public Access

Author manuscript

Mol Imaging Biol. Author manuscript; available in PMC 2017 October 16.

Published in final edited form as:

Mol Imaging Biol. 2016 December ; 18(6): 924–934. doi:10.1007/s11307-016-1007-0.

Utility of [^{18}F]FSPG PET to Image Hepatocellular Carcinoma: First Clinical Evaluation in a US Population

Gina Kavanaugh[1,2,3], **Jason Williams**[1,2,3], **Andrew Scott Morris**[2], **Michael L. Nickels**[1,2,3], **Ronald Walker**[2,4], **Norman Koglin**[5], **Andrew W. Stephens**[5], **M. Kay Washington**[6], **Sunil K. Geevarghese**[7], **Qi Liu**[8,9], **Dan Ayers**[10], **Yu Shyr**[9,10,11], and **H. Charles Manning**[1,2,3,4,12,13,14,15,16]

[1]Vanderbilt University Institute of Imaging Science, Vanderbilt University Medical Center, Nashville, TN, 37232, USA

[2]Department of Radiology and Radiological Sciences, Vanderbilt University Medical Center, Nashville, TN, 37232, USA

[3]Vanderbilt Center for Molecular Probes, Vanderbilt University Medical Center, Nashville, TN, 37232, USA

[4]Vanderbilt-Ingram Cancer Center, Vanderbilt University Medical Center, Nashville, TN, 37232, USA

[5]Piramal Imaging GmbH, Berlin, Germany

[6]Department of Pathology, Vanderbilt University Medical Center, Nashville, TN, 37232, USA

[7]Department of Surgery, Vanderbilt University Medical Center, Nashville, TN, 37232, USA

[8]Department of Biomedical Informatics, Vanderbilt University School of Medicine, Nashville, TN, 37232, USA

[9]Center for Quantitative Sciences, Vanderbilt University School of Medicine, Nashville, TN, 37232, USA

[10]Department of Biostatistics, Vanderbilt University School of Medicine, Nashville, TN, 37232, USA

[11]Department of Cancer Biology, Vanderbilt University School of Medicine, Nashville, TN, 37232, USA

[12]Program in Chemical and Physical Biology, Vanderbilt University Medical Center, Nashville, TN, 37232, USA

[13]Department of Neurosurgery, Vanderbilt University Medical Center, Nashville, TN, 37232, USA

Correspondence to: H. Manning; henry.c.manning@vanderbilt.edu.

Compliance with Ethical Standards

Conflict of Interest

Norman Koglin and Andrew W. Stephens are employees of Piramal Imaging GmbH and are co-inventors of the compound under investigation and/or have ownership interests in Piramal Imaging.

[14]Vanderbilt Institute of Chemical Biology, Vanderbilt University Medical Center, Nashville, TN, 37232, USA

[15]Department of Biomedical Engineering, Vanderbilt University, Nashville, TN, 37232, USA

[16]Department of Chemistry, Vanderbilt University, Nashville, TN, 37232, USA

Abstract

Purpose—Non-invasive imaging is central to hepatocellular carcinoma (HCC) diagnosis; however, conventional modalities are limited by smaller tumors and other chronic diseases that are often present in patients with HCC, such as cirrhosis. This pilot study evaluated the feasibility of (4*S*)-4-(3-[^{18}F]fluoropropyl)-L-glutamic acid ([^{18}F]FSPG) positron emission tomography (PET)/X-ray computed tomography (CT) to image HCC. [^{18}F]FSPG PET/CT was compared to standard-of-care (SOC) magnetic resonance imaging (MRI) and CT, and [^{11}C]acetate PET/CT, commonly used in this setting. We report the largest cohort of HCC patients imaged to date with [^{18}F]FSPG PET/CT and present the first comparison to [^{11}C]acetate PET/CT and SOC imaging. This study represents the first in a US HCC population, which is distinguished by different underlying comorbidities than non-US populations.

Procedures—x_{C-} transporter RNA and protein levels were evaluated in HCC and matched liver samples from The Cancer Genome Atlas (n = 16) and a tissue microarray (n = 83). Eleven HCC patients who underwent prior MRI or CT scans were imaged by [^{18}F]FSPG PET/CT, with seven patients also imaged with [^{11}C]acetate PET/CT.

Results—x_{C-} transporter RNA and protein levels were elevated in HCC samples compared to background liver. Over 50 % of low-grade HCCs and ~70 % of high-grade tumors exceeded background liver protein expression. [^{18}F]FSPG PET/CT demonstrated a detection rate of 75 %. [^{18}F]FSPG PET/CT also identified an HCC devoid of typical MRI enhancement pattern. Patients scanned with [^{18}F]FSPG and [^{11}C]acetate PET/CT exhibited a 90 and 70 % detection rate, respectively. In dually positive tumors, [^{18}F]FSPG accumulation consistently resulted in significantly greater tumor-to-liver background ratios compared with [^{11}C]acetate PET/CT.

Conclusions—[^{18}F]FSPG PET/CT is a promising modality for HCC imaging, and larger studies are warranted to examine [^{18}F]FSPG PET/CT impact on diagnosis and management of HCC. [^{18}F]FSPG PET/CT may also be useful for phenotyping HCC tumor metabolism as part of precision cancer medicine.

Keywords

PET; FSPG; HCC; Cancer imaging

Introduction

Hepatocellular carcinoma (HCC) is the most common primary malignancy of the liver and ranks fifth and seventh among men and women, respectively, in worldwide cancer incidence [1]. Though HCC has historically affected the continent of Asia disproportionately (~80 % of cases), the American Cancer Society estimates the diagnosis of greater than 39,000 new cases of primary liver cancer in the USA this year, with approximately 75 % of these being

HCC [2]. Additionally, both the incidence of liver cancer and liver cancer-associated deaths are increasing [1, 2].

Liver disease and cirrhosis due to hepatitis B (HBV), hepatitis C (HCV), and non-alcoholic steatohepatitis (NASH) are the greatest contributors to the development of HCC [3]. Surgery is the best treatment option for HCC, and patients are evaluated by using “Milan” criteria (single tumor, diameter ≤5 cm; ≤3 tumors, each diameter ≤3 cm) [4]. However, the clinical application of Milan criteria is limited by the sensitivities of X-ray computed tomography (CT) and magnetic resonance imaging (MRI), which are diminished by the architectural distortions within the liver that are characteristic of cirrhosis [5]. While the overall sensitivities of CT and MRI in the setting of HCC are typically reported in the 60–70 % range, smaller lesions (1–2 cm) can exhibit a much lower rate of detection (40 %) [6–8]. The specificity of CT and MRI are also limited, as several benign conditions in the liver, often associated with cirrhosis, can be challenging to distinguish from neoplasia without biopsy or extensive imaging follow-up [7]. Therefore, improved ways to image HCC could enable improved diagnosis and staging, both of which would lead to improved clinical care for these patients.

The diverse background in which HCC develops, without a predictable trajectory of mutations leading to tumorigenesis, makes molecular imaging, such as positron emission tomography (PET), an attractive approach for this disease. To date, the role of PET imaging in HCC is not well established. Collective experience with the most widely used PET tracer in oncology, 2-deoxy-2-[^{18}F]fluoro-D-glucose ([^{18}F]FDG), a probe that measures glucose utilization, has been variable. Uptake of [^{18}F]FDG in HCC appears to be limited primarily to high-grade/poorly - differentiated lesions and demonstrates a modest overall sensitivity of lesion detection of 50 % [9, 10]. In contrast, [^{11}C]acetate, another tracer explored for HCC detection that takes advantage of the pathway that synthesizes free fatty acids, accumulates primarily in low-grade/well-differentiated HCC lesions [4, 10]. Dual-tracer [^{18}F]FDG and [^{11}C]acetate PET studies have shown encouraging results, with one study reporting overall sensitivity and specificity of greater than 90 % in orthotopic liver transplantation (OLT) patients with cirrhosis [8]. However, there are several important drawbacks of dual-tracer studies that limit routine adoption, including additional procedural complexity, greater cost, and greater risk to patients and clinical personnel. Additionally, the short half-life of [^{11}C]acetate adds further technical challenges. Thus, an alternative PET tracer with a suitable half-life for distribution that exhibits a high rate of HCC detection and sensitivity for both well-differentiated and poorly - differentiated tumors would be very clinically attractive.

Pilot studies indicate that (4*S*)-4-(3-[^{18}F]fluoropropyl)-L-glutamic acid ([^{18}F]FSPG, INN: florilglutamic acid (^{18}F)), a novel F-18-labeled radiotracer designed for PET imaging of tumors, accumulates in HCC lesions as well [11]. [^{18}F]FSPG is taken up by cells through the system x_{C-} transporter, which is commonly activated in many cancer types. A recent study in South Korea evaluated [^{18}F]FSPG in a small group of patients ($n = 5$) with confirmed HCC. Those patients each had a prior [^{18}F]FDG PET/CT scan [11]. Accumulation of [^{18}F]FSPG was detected in all patients with HCC (5/5), whereas [^{18}F]FDG PET showed hypermetabolic lesions in three of five patients and isometabolic lesions in the

remaining two, yielding a qualitative sensitivity of 60 % for [^{18}F]FDG and 100 % for [^{18}F]FSPG in this small cohort. Notably, [^{18}F]FSPG accumulated in both moderately- and poorly - differentiated HCC. In dually positive tumors, [^{18}F]FSPG and [^{18}F]FDG achieved similar levels of uptake, yet accumulation of [^{18}F]FSPG was lower in background liver, which enabled improved imaging contrast. Though this study was too small to draw definitive conclusions, this study suggested that [^{18}F]FSPG has the potential to detect HCC of varying degrees of differentiation and is a promising tracer for HCC detection. In this study, we further examine the ability of [^{18}F]FSPG PET to detect HCC lesions in a Western population and compare [^{18}F]FSPG uptake with [^{11}C]acetate. These results show that HCC tumor tissue expresses increased RNA and protein levels of the x_{C-} transporter, increasing uptake of [^{18}F]FSPG, compared to normal liver tissue. We found that [^{18}F]FSPG PET detected a small HCC lesion that was difficult to detect by MRI. Additionally, [^{18}F]FSPG PET exhibited a higher detection rate for HCC lesions than [^{11}C]acetate, with a much lower level of tracer uptake in background liver. Overall, this study indicates that [^{18}F]FSPG PET may be useful for HCC detection and patient management.

Materials and Methods

Patient Population and Selection

Vanderbilt University Medical Center (VUMC)'s Institutional Review Board (IRB) approved this study under the purview of the Food and Drug Administration investigational new drug (IND) applications 124202 ([^{18}F]FSPG) and 120704 ([^{11}C]acetate). The clinical trial was registered in ClinicalTrials.gov (identifier NCT02379377). The study was approved by Vanderbilt's IRB and the Vanderbilt-Ingram Cancer Center (VICC) Scientific Review Committee. Written informed consent was obtained from all patients prior to participation in the study. Patients scheduled for OLT or liver resection were considered for participation. Inclusion criteria for eligible participants included the diagnosis of HCC with one or more of the following: (1) a liver mass ≥1 cm with arterial phase contrast enhancement and early washout on subsequent phases by CT or MRI, (2) suggestive imaging findings, or (3) tumor confirmed by arteriography and a prior conventional imaging and staging CT (multiphase) or MRI before initiation of the investigation PET studies. Exclusion criteria included: (1) patients under 18 years of age; (2) patients with a known prior malignancy who received systemic therapy within 5 years, except basal cell carcinoma of the skin, carcinoma in situ of the cervix, and prior HCC; (3) pregnant and breastfeeding patients; (4) patients with poorly controlled diabetes mellitus; (5) patients with a known infiltrative variant of HCC; and (6) prior treatment within 1 year for HCC. Eleven patients were prospectively enrolled and imaged with [^{18}F]FSPG or [^{18}F]FSPG and [^{11}C]acetate between March 2015 and March 2016.

Radiochemistry

[^{18}F]FSPG and [^{11}C]acetate were produced by the Vanderbilt Center for Molecular Probes Radiochemistry Core Laboratory in accordance with the Chemistry, Manufacturing, and Control (CMC) sections of the INDs referenced above. Tracers met all USP <823> requirements for sterile, injectable PET radiopharmaceuticals. The tracers used for this PET study were previously evaluated in humans at VUMC and other sites, with no adverse side

effects, such as anaphylactic reactions, allergic reactions, or mortality or morbidity, observed. The total mass of radiopharmaceutical administered in this study was in the subpharmacological amount and was therefore expected to have no physiologic effect on the patient or tumor. Production of [^{18}F]FSPG employed radiolabeling of the protected precursor di-*tert*-butyl-(2*S*,4*S*)-2-(3-((naphthalen-2-ylsulfonyl)oxy)propyl)-4-(tritylamino)pentanedioate) with cyclotron-generated [^{18}F]fluoride in the presence of K^+-$K_{2.2.2}/K_2CO_3$. After acidic deprotection, neutralization, and aqueous dilution, the tracer was purified over SPE cartridges and finally formulated for i.v. injection by passing the solution through a sterile filter. The synthesis was performed within an automated synthesis module (GE MX Reaction Module) in a lead-shielded hot cell. The production methods, sterile filtration, and formulation allowed for the production of a sterile and pyrogen-free solution ready for injection. A small aliquot was removed for analysis to confirm the quality of the final product solution. The radiochemical synthesis of sodium [^{11}C]acetate began with [^{11}C]CO_2 gas, which was made by proton irradiation of a high-pressure gas target containing 99 % nitrogen and 1 % oxygen gas. The [^{11}C]CO_2 was then purified by trapping on activated molecular sieves (4 Å) followed by heating with a flow of pure nitrogen to release the [^{11}C]CO_2 gas. The [^{11}C]CO_2-containing gas was bubbled directly into a THF-diluted solution of methylmagnesium chloride (3.0 M). Upon completion of the [^{11}C]CO_2 delivery, the remaining methylmagnesium chloride was quenched by using a dilute solution of sulfuric acid. The reaction mixture was then transferred through a SCX cartridge, a SAX cartridge, and an IC-OH cartridge. All of the purification cartridges and the reaction vessel were then washed with water. The IC-OH cartridge was then isolated, and using saline, the sodium [^{11}C]acetate was eluted from the cartridge through a 0.22-μm sterilizing filter and into the final vial. The concentration was then adjusted to not exceed 50 mCi/ml, and a small aliquot was removed for analysis to confirm the quality of the final product solution. All released doses exceeded 266 Ci/mmol with radiochemical purity greater than 90 % for [^{18}F]FSPG and greater than 95 % for [^{11}C]acetate.

PET/CT Protocol

Patients were instructed to fast (nothing by mouth except for water and some medications) for at least 6 h prior to imaging and to refrain from smoking on the day of the imaging procedure.

[^{18}F]FSPG PET/CT only or both [^{18}F]FSPG PET/CT and [^{11}C]acetate PET/CT images were collected in patients diagnosed with HCC who had previously undergone SOC CT or MRI imaging and prior to liver resection surgery, OLT, or interventional radiology therapy. Images were acquired on a GE Discovery STE PET/CT scanner with emission imaging in 3D mode with scatter correction. CT scans obtained for attenuation correction were low dose. [^{11}C]acetate PET/CT was collected on the same day as the [^{18}F]FSPG PET/CT. In this scenario, [^{11}C]acetate PET/CT was collected prior to [^{18}F]FSPG PET/CT, with approximately 2 h in between the injections. [^{11}C]acetate imaging was conducted similarly to previously reported methods [12]. Twenty minutes following intravenous administration of [^{11}C]acetate (7.4 MBq/kg body weight), the patient was positioned on the imaging table, and a whole body (vertex of the skull to mid-thigh) transmission CT scan acquired (~90 s) followed by a whole body (vertex of the skull to mid-thigh) PET scan at 4 min/bed position

(~40 min). For [^{18}F]FSPG PET, a dynamic study was conducted. Patients were positioned in the PET/CT scanner, and following intravenous injection of 300 MBq (8.1 mCi) of [^{18}F]FSPG, the PET scan was performed during two time intervals. Time interval number 1 was from 0 to 25 min and time interval number 2 from 60 to 95 min post injection. During each interval, a CT transmission scan was collected for attenuation correction. For time interval 1, one image was collected over the liver with tracer injection as follows: 30 s, 30 s, 1 min, 2 min, 2 min, 30 s, 30 s, 1 min, 2 min, and 2 min per frame. During interval 2, multiple consecutive images were collected from skull to mid-thigh at 4 min per bed position. Patients were asked to void their urinary bladder immediately after their first scan, as well as before and following the second interval.

Image Analysis

The research SOC MRI and CT and research PET/CT images were independently evaluated by an experienced nuclear medicine physician. Quantitative measurements of uptake were in accordance with PETCIST criteria as described by Wahl et al. [13], with anatomic measurements as described by RECIST 1.1 [14]. Full access to prior imaging (CT, MRI, and ultrasound) was allowed. There was one observer, with 15-years experience with PET/CT and 35+ years of experience in medical imaging, with extensive experience in investigative imaging, and with American board certifications in both diagnostic radiology and nuclear medicine. The observer was not blinded to pathology results when they were available. Sixty minute [^{18}F]FSPG scans were used to determine standardized uptake values (SUVs). Maximum standardized uptake values (SUV_{max}) were normalized to lean body mass and measured with a 1 ml spherical region of interest over the area of greatest uptake in the tumor being measured. Background uptake (SUV_{max}) of normal organs was obtained by using a 3 cm diameter spherical region of interest. Normal liver uptake was measured in the peripheral right lobe, with care to avoid inclusion of major vascular structures, anatomic abnormalities, or areas of tumor. These measurements were performed by using Xeleris 3.0 workstation hardware and software from GE Healthcare, Waukesha, MI, USA. Maximum intensity projection images and fusion of axial PET images with accompanying CT were performed by using OsiriX (v5.5.2, Pixmeo, Geneva, Switzerland). For comparison, [^{11}C]acetate PET and [^{18}F]FSPG PET images were windowed from SUV 0–10, as this encompassed the range of SUV_{max} measurements obtained in liver tumor ROIs from each tracer for all patients (see Table 1). For comparison of [^{18}F]FSPG and [^{11}C]acetate SUVs, a non-parametric paired test was performed.

The Cancer Genome Atlas RNA-Seq Analysis

RNA expression levels of the x_{C-} transporter (gene symbol *SLC7A11*) were obtained for stage 1 HCC and matched normal liver samples from The Cancer Genome Atlas (TCGA). A paired *t* test was performed to assess the statistical significance of the observed differential expression between HCC and normal samples.

Tissue Microarray and Immunohistochemistry

The tissue microarray (TMA) was created by using duplicate 1 mm cores from 83 HCC tumors and matched background liver. All cases were from hepatectomies performed for liver transplantation or from partial hepatectomy specimens. Etiology of underlying liver

disease was chronic hepatitis C with or without alcohol abuse (42), chronic hepatitis B with or without alcohol abuse or concomitant hepatitis C infection (9), alcohol abuse without viral infection (4), hemochromatosis (1), non-alcoholic fatty liver disease (5), and no or unknown liver disease (22). TMAs were sectioned onto slides and immunohistochemistry (IHC) to detect the x_{C-} transporter performed. First, antigen retrieval was carried out in pH 6.0 citrate buffer in a pressure cooker at 104 °C for 20 min and then cooled for 10 min at room temperature. Samples were then quenched in 0.02 % H_20_2 with sodium azide for 5 min, blocked in serum-free protein block Dako X0909 for 15 min, and incubated in primary antibody (xCT antibody; Novus) at 1:2000 dilution for 60 min. Detection was carried out by incubating for 20 min in Dako Envision plus HRP-labeled polymer and then incubating with chromogen DAB for 5 min. Samples were determined to be positive or negative for x_{C-} expression, and categorical variables (e.g., tumor grade) were summarized in frequency tables and compared among important subgroups by using the chi-squared test.

Pathology

When possible, diagnosis of HCC lesions was confirmed by CT-guided needle biopsy. The explanted liver sections shown in Fig. 4d for patient 5 were obtained following a right lobe, partial hepatectomy. The liver was serially sectioned in slices measuring 5 mm or less. Gross examination of liver explant specimens was performed by an expert GI pathologist for final determination of HCC status of suspected lesions.

Results

x_{C-} transporter Expression Is Elevated in HCC Tumor Tissue

The PET tracer [^{18}F]FSPG takes advantage of increased x_{C-} transporter activity, which is associated to part of the truncated tricarboxylic acid (TCA) cycle often utilized as an alternative metabolic pathway in tumor cells (Fig. 1). To determine whether HCC tumors have elevated RNA levels of the x_{C-} transporter (gene symbol *SLC7A11*), we queried RNA-Seq data from TCGA to compare HCC and normal liver tissue. Supporting our hypothesis that [^{18}F]FSPG PET/CT may be useful in the detection of low-grade HCC, we observed that over 80 % of stage 1 HCCs exhibited *SLC7A11* expression that exceeded background liver in matched specimens (Fig. 2, $n = 16$, $p < 0.01$), with over half of the specimens exhibiting an expression difference that exceeded 2-fold. We also evaluated x_{C-} protein levels by IHC in normal liver and HCC tumors by using a TMA of 83 patient specimens (Fig. 3). Similar to the RNA-Seq data, approximately 70 % of the HCCs evaluated were positive for x_{C-} transporter expression by IHC analysis. Immunoreactivity of background, non-tumor liver was negligible, yet tumors exhibited robust staining that was confined to the tumor cells and was primarily localized to the cell membrane. While a greater proportion of higher grade (3 and 4) HCCs were positive for SLC7A11, we were encouraged that approximately half of the low-grade tumors exhibited robust staining. These data showing elevated x_{C-} in HCC tumors suggest that [^{18}F]FSPG is likely to be taken up by these tumor cells and has potential for HCC detection.

[18F]FSPG and [11C]Acetate PET Imaging

[18F]FSPG uptake was examined in a cohort of 11 patients with a diagnosis of HCC and compared [18F]FSPG PET with [11C]acetate PET in 7 of the 11 patients. In all patients studied, [18F]FSPG and [11C]acetate were well-tolerated, with no observable side effects of any kind. Patients were observed for changes in subjective state of health or any untoward reactions, such as allergic reactions. Patient characteristics and imaging results are summarized in Table 1. Patients ranged in age from 38 to 77, with the median age of study participants being 62. Four of the 11 patients accrued exhibited more than one HCC lesion, while seven had only one. The lesions ranged in largest diameter from 1.2 to 5.1 cm, with the median longest diameter being 3.0 cm. Seven of the 11 patients (64 %) evaluated exhibited clinical cirrhosis. Encouragingly, 12 of 16 HCC lesions (identified by SOC MRI or CT) evaluated in the 11 patients exhibited significant [18F]FSPG accumulation that exceeded background liver and were easily detectable, rendering a tumor detection rate of 75 % (12/16) for [18F]FSPG PET/CT in this setting. SUV values ranged from 0.7 to 9.2 for HCC tumors, while SUV values for background liver were much lower, ranging from 0.5 to 1.9. It was not obvious that the presence or absence of cirrhosis affected the background liver SUV, as patient 6 (cirrhosis) and patients 5 and 7 (no cirrhosis) exhibited the lowest background liver uptake, while patient 3 (no cirrhosis) exhibited one of the highest SUV background values. Regardless, the low background uptake appeared to be a major contributor to the promising tumor-to-liver background ratios achieved in detected HCC tumors. Among patients whose HCC tumor differentiation status was known (Table 1), no obvious trend emerged for [18F]FSPG uptake and tumor differentiation in this pilot study, suggesting that [18F]FSPG may be useful for detection of a variety of HCC lesions.

Figure 4 shows representative [18F]FSPG PET images, 60 min post administration, from patient 5. The typical biodistribution pattern for [18F]FSPG was observed in this patient, with retained activity observed in the oral cavity, pancreas, fundus of the stomach, and kidneys, with evidence of urinary excretion (Fig. 4a). Background liver accumulation was modest in this patient (SUV 0.5). Two lesions were easily detected by [18F]FSPG PET/CT in this patient, with one being a larger HCC (4.7 cm, SUV 9.2; Fig. 4a, b, Table 1) that was readily identified on SOC MRI (Fig. 4c, left image). Importantly, however, a much smaller satellite lesion (1.2 cm, SUV 3.8; Fig. 4a, b, Table 1) was also easily detected by [18F]FSPG PET, an HCC later confirmed at resection, that was suspicious for HCC by SOC MRI but significantly less obvious (Fig. 4c, right image). Liver explant analysis following resection (Fig. 4d) subsequently confirmed that both lesions were HCC. The detection of the smaller satellite lesion which was less easily detected by MRI indicated that [18F]FSPG PET may be useful for detection of small tumors not easily seen by SOC imaging techniques.

In addition to [18F]FSPG PET, seven patients were also scanned with [11C]acetate PET. Previous studies indicated that [11C]acetate primarily detects low-grade/well-differentiated HCC lesions. We sought to determine whether [18F]FSPG PET could detect a wider range of HCC lesions than [11C]acetate PET (Table 1). Of five of the seven patients scanned, [18F]FSPG PET exhibited a higher tumor-to-liver background value than, and for one patient equal to, [11C]acetate PET. Only one patient, patient 2, demonstrated greater [11C]acetate uptake than [18F]FSPG (Fig. 5). Of the patients exhibiting higher [18F]FSPG uptake,

[^{18}F]FSPG PET tumor-to-liver background ratios ranged from 1.5-fold to 3.2-fold higher than [^{11}C]acetate (Table 1). Absolute uptake of [^{18}F]FSPG was lower than absolute [^{11}C]acetate uptake ($p = 0.0383$); however, the lower levels of background liver uptake of [^{18}F]FSPG ($p = 0.0016$) resulted in greater tumor-to-liver background ratios (Table 1). Of the 10 lesions examined in the seven patients, 9 were detected with [^{18}F]FSPG PET for a detection rate of 90 %, while 7 were detected with [^{11}C]acetate (detection rate of 70 %). In patients 1, 7, and 11, the HCC lesions were detected by [^{11}C]acetate PET; however, tumor to background was greater with [^{18}F]FSPG PET (Table 1). In patient 10, who had three HCC lesions, only one lesion was detected with [^{11}C]acetate, while the other two lesions exhibited non-significant accumulations (Table 1, Fig. 6). However, [^{18}F]FSPG PET detected all three lesions. Additionally, for lesions detected by both [^{18}F]FSPG and [^{11}C]acetate, [^{18}F]FSPG PET exhibited much lower levels of background in the liver with SUVs ranging from 0.5 to 1.9, while background liver SUVs ranged from 3.2 to 6.1 with [^{11}C]acetate PET. Overall, lower background levels contributed to better detection of lesions by [^{18}F]FSPG.

Discussion

With the fifth and seventh highest cancer incidences in men and women, respectively, HCC is a major health concern both in the US and worldwide. Currently, CT and MRI imaging are used to diagnose HCC; however, these imaging techniques can be confounded in patients who have cirrhosis due to structural distortions caused by the disease. As cirrhosis is a common risk factor leading to the development of HCC, alternative imaging methods such as PET could be particularly useful for HCC diagnosis. Additionally, CT and MRI imaging detection rates are much lower (40 %) for smaller lesions, which PET imaging might improve.

PET is an especially useful imaging technique, as tracers are designed specifically to target molecular pathways. The [^{18}F]FSPG PET tracer employed in this study targets a pathway used by many tumor types (Fig. 1). As a result of the truncated TCA cycle, glutamine and glutamate are often major metabolic and anabolic substrates of tumor cells, in parallel or even in lieu of glucose-derived metabolites like pyruvate. As part of this alternate pathway, L-glutamine is taken up via the ASCT2 transporter and processed into L-glutamate, which is then utilized by the truncated TCA cycle. The system x_{C-} transporter, a glutamate-cystine exchanger [15], also transports L-glutamate out of the cell and L-cystine into the cell in a rate-limiting fashion, thus providing precursors for glutathione (GSH) biosynthesis. [^{18}F]FSPG, which functions as a cystine mimetic, is specifically taken up via the system x_{C-} transporter. Our RNA-Seq and IHC analyses indicated that HCC tumor tissues have elevated expression levels of the x_{C-} transporter in comparison to non-cancerous background liver (Figs. 2 and 3). These data suggest that HCC cells may rely on alternative metabolism provided by the truncated TCA cycle, in the respect that [^{18}F]FSPG reflects glutamine metabolism as related to intracellular glutamate pools replenished from transported glutamine.

A number of groups have examined the metabolic characteristics of HCC and found elevated serum levels of glutamate and reduced glutamine levels in patients with HCC [16–20]. This finding is consistent with the truncated TCA cycle, as the tumor cells salvage extracellular

glutamine to produce glutamate, which can then be shuttled into the TCA cycle or exported from the cell via the x_{C-} transporter to exchange for L-cystine, a substrate required for glutathione biosynthesis and cellular redox maintenance. Importantly, glutamate and glutathione metabolism have been shown to be closely correlated with the development and carcinogenesis of HCC. A study comparing the metabolic profile of non-cancerous liver and HCC tumors showed increased levels of tumor cell glutamine and glutathione in HCC tumors [21]. Thus, glutamine and glutamate may play a major role in the development, progression, and maintenance of HCC. Additionally, cystine, which is imported into the cell by the x_{C-} transporter, is utilized as a precursor for glutathione synthesis. Redox maintenance is enabled through a constant supply of glutathione and is critical for tumor cells to protect against the toxic accumulation of reactive oxygen species. A constant supply of glutathione may enhance tumor survival, particularly during therapeutic interventions [22], and therefore may contribute to HCC development and progression. A non-invasive imaging method that provides a surrogate biological metric for assessing glutamate/glutamine metabolism of HCC tumors has the potential to enhance HCC diagnosis. Additionally, characterization of glutamate and glutamine metabolism in HCC tumors may be useful for determining the most effective treatments for lesion response.

A previous study evaluated [^{18}F]FSPG PET in patients with breast (n = 5) and lung (n = 10) cancer, where the tracer exhibited a promising detection rate of tumors with x_{C-} transporter activity [22]. Baek et al. reported that elevated glycolytic activity and uptake of [^{18}F]FSPG appeared to be correlated in lung cancer, but a similar relationship was not observed in breast cancer [22]. IHC analyses of imaging-matched human pathology samples from this study showed significant correlation between [^{18}F]FSPG uptake and protein expression of both the SLC7A11 subunit of the x_{C-} heterodimer and CD44. In breast tumor samples specifically, IHC showed that the absence of CD44 correlated with low signal from [^{18}F]FSPG-PET, even if the SLC7A11 subunit was present, suggesting the importance of CD44 co-expression for system x_{C-} function in breast cancer [22]. This relationship has not been established in other solid tumors. Future studies examining specific levels of x_{C-} transporter and CD44 expression levels in HCC tumors in correlation with [^{18}F]FSPG uptake will be important for a more complete understanding of HCC tumors and improved detection and treatment methods.

Here, we evaluated the ability of [^{18}F]FSPG PET to detect HCC lesions. We found [^{18}F]FSPG uptake in 12 of 16 lesions examined, for an overall detection rate of 75 %. Tumor SUV values were much higher than background livers (0.7–9.2 vs. 0.5–1.9, respectively), resulting in strong HCC tumor detection. Additionally, [^{18}F]FSPG PET easily detected a very small lesion in patient 5 that was more difficult to detect by SOC MRI. Although further studies in a larger cohort are needed, this data indicates that [^{18}F]FSPG PET may be useful for detection of small HCC tumors, which would assist physicians in identifying lesions at earlier stages and allow for earlier treatments to improve tumor response and patient survival.

Clinical comparisons between [^{11}C]acetate and [^{18}F]FDG PET in HCC have previously been examined. An early study using [^{11}C]acetate PET reported a considerable improvement in the sensitivity for lesion detection compared to [^{18}F]FDG (87.3 vs. 47.3 %) [10]; these

statistics were confirmed in subsequent studies [8]. Interestingly, several studies observed that [^{18}F]FDG and [^{11}C]acetate accumulate in tumors discordantly; [^{11}C]acetate tends to accumulate in low-grade/well-differentiated HCC, whereas [^{18}F]FDG accumulates in high-grade/poorly - differentiated tumors [10]. Biologically, this implies that as HCC becomes more malignant and dedifferentiated, the biochemical substrates for growth shift. Importantly, the majority of smaller HCCs tend to be well-differentiated, suggesting that [^{11}C]acetate PET may play a greater role in evaluating patients with early stage disease [3]. Unfortunately, dual-tracer detection is not ideal due to cost and procedural complexity, in addition to the difficulties associated with the short half-life of [^{11}C]acetate. Therefore, we sought to determine whether [^{18}F]FSPG PET could be utilized as a single tracer to better detect HCCs at various stages of differentiation.

Patients with HCC were imaged with both [^{18}F]FSPG and [^{11}C]acetate PET to determine whether [^{18}F]FSPG PET could improve HCC detection. Indeed, we observed that 9 of the 10 tumors examined were detected by [^{18}F]FSPG PET, resulting in a 90 % detection rate. However, only 7 of the 10 tumors were detectable by [^{11}C]acetate PET. In two patients, [^{18}F]FSPG uptake was observed in all tumors detected by SOC imaging, whereas [^{11}C]acetate uptake was detected in only a subset of the tumors. Further evaluation of tumors indicated that the average [^{11}C]acetate uptake was slightly significantly higher than [^{18}F]FSPG uptake (p value = 0.0383). However, the superiority of [^{18}F]FSPG detection likely stems from the difference in background liver uptake; [^{18}F]FSPG uptake was significantly lower than [^{11}C]acetate (p value = 0.0016) and contributes to the greater tumor to liver ratio observed with [^{18}F]FSPG. In tumors detected by both tracers, the much lower background levels of [^{18}F]FSPG uptake contributed to the improved detection of tumors compared to [^{11}C]acetate. Overall, these data indicate that [^{18}F]FSPG PET has potential for detection of HCC tumors by PET, which could also potentially improve detection of small tumors leading to early treatment and improved patient outcome.

A number of questions remain warranting further examination of [^{18}F]FSPG PET for HCC detection and further define its clinical utility. [^{18}F]FSPG PET did not detect tumors in patients 2, 8, and 9. To determine why [^{18}F]FSPG PET does not detect all tumors, evaluation of x_{C-} transporter expression (in addition to CD44 expression) and clinical follow-up of the patients should be carried out. Our expression level analyses indicate that 20–30 % of HCC tumors did not express the x_{C-} transporter. These patients may have lower levels of [^{18}F]FSPG uptake due to low expression of the x_{C-} transporter and therefore less dependence on the alternative metabolism pathway, which may guide these patients to other distinct therapies. Additionally, [^{18}F]FSPG uptake should be examined in benign liver tumors to determine whether [^{18}F]FSPG can differentiate HCC liver tumors specifically. A more complete understanding of the cellular mechanisms affecting HCC growth and [^{18}F]FSPG uptake will lead to better detection of all HCC lesions and improved treatment. Additionally, we hypothesize that [^{18}F]FSPG may be useful as a predictor of treatment response, by utilizing it to understand the metabolic characteristics of HCC lesions. Future studies examining [^{18}F]FSPG uptake and tumor response to treatment may also be beneficial for further enhancing treatment and management of HCC tumors.

Conclusion

The diagnostic potential of [^{18}F]FSPG is promising. [^{18}F]FSPG PET detects HCC lesions equivalent to or better than SOC MRI and CT imaging. It could potentially be used to complement MRI and CT where PET is more sensitive for the detection of smaller lesions and lesions confounded by background cirrhosis. [^{18}F]FSPG PET exhibited a higher detection rate for HCC lesions compared to [^{11}C]acetate PET and should be further validated in a larger population of patients. Additionally, a strength of [^{18}F]FSPG PET is the reflection of glutamate/glutathione metabolism, which could be utilized to characterize the metabolic profile of HCC lesions and be used to predict patient response to therapies.

Acknowledgments

This work was supported by National Institutes of Health grant 6P30CA068485, Vanderbilt University institutional support to the Center for Molecular Probes, and a Vanderbilt Trans-Institutional Programs Award. Piramal Imaging provided a portion of the radiochemistry materials used in this study. The authors wish to thank Dr. Michael Schulte for assistance with creating the molecular pathway in Fig. 1.

References

1. Ferlay J, Shin HR, Bray F, et al. Estimates of worldwide burden of cancer in 2008: GLOBOCAN 2008. International journal of cancer Journal international du cancer. 2010; 127:2893–2917. [PubMed: 21351269]
2. Cancer Facts & Figures. Atlanta: America Cancer Society; 2016.
3. El-Serag HB. Hepatocellular carcinoma. New Engl J Med. 2011; 365:1118–1127. [PubMed: 21992124]
4. Mazzaferro V, Regalia E, Doci R, et al. Liver transplantation for the treatment of small hepatocellular carcinomas in patients with cirrhosis. New Engl J Med. 1996; 334:693–699. [PubMed: 8594428]
5. Llovet JM, Schwartz M, Mazzaferro V. Resection and liver transplantation for hepatocellular carcinoma. Semin Liver Dis. 2005; 25:181–200. [PubMed: 15918147]
6. Sangiovanni A, Manini MA, Iavarone M, et al. The diagnostic and economic impact of contrast imaging techniques in the diagnosis of small hepatocellular carcinoma in cirrhosis. Gut. 2010; 59:638–644. [PubMed: 19951909]
7. Yu NC, Chaudhari V, Raman SS, et al. CT and MRI improve detection of hepatocellular carcinoma, compared with ultrasound alone, in patients with cirrhosis. Clin Gastroenterol Hepatol. 2011; 9:161–167. [PubMed: 20920597]
8. Cheung TT, Ho CL, Lo CM, et al. ^{11}C-acetate and ^{18}F-FDG PET/CT for clinical staging and selection of patients with hepatocellular carcinoma for liver transplantation on the basis of Milan criteria: surgeon's perspective. J Nucl Med. 2013; 54:192–200. [PubMed: 23321459]
9. Jadvar H. Hepatocellular carcinoma and gastroenteropancreatic neuroendocrine tumors: potential role of other positron emission tomography radiotracers. Semin Nucl Med. 2012; 42:247–254. [PubMed: 22681673]
10. Grassi I, Nanni C, Allegri V, et al. The clinical use of PET with (11)C-acetate. Am J Nucl Med Mol imaging. 2012; 2:33–47. [PubMed: 23133801]
11. Baek S, Mueller A, Lim YS, et al. 4S)-4-(3-18F-fluoropropyl)-L-glutamate for imaging of xC transporter activity in hepatocellular carcinoma using PET: preclinical and exploratory clinical studies. J Nucl Med. 2013; 54:117–123. [PubMed: 23232273]
12. Ho CL, Cheung MK, Chen S, et al. [18F]fluoroacetate positron emission tomography for hepatocellular carcinoma and metastases: an alternative tracer for [11C]acetate? Mol Imaging. 2012; 11:229–239. [PubMed: 22554487]

13. Wahl RL, Jacene H, Kasamon Y, et al. From RECIST to PERCIST: evolving considerations for PET response criteria in solid tumors. J Nucl Med. 2009; 50(Suppl 1):122S–150S. [PubMed: 19403881]
14. Schwartz LH, Bogaerts J, Ford R, et al. Evaluation of lymph nodes with RECIST 1.1. Eur J Cancer. 2009; 45:261–267. [PubMed: 19091550]
15. Koglin N, Mueller A, Berndt M, et al. Specific PET imaging of xC-transporter activity using a (1) (8)F-labeled glutamate derivative reveals a dominant pathway in tumor metabolism. Clin Cancer Res. 2011; 17:6000–6011. [PubMed: 21750203]
16. Fitian AI, Nelson DR, Liu C, Xu Y, Ararat M, Cabrera R. Integrated metabolomic profiling of hepatocellular carcinoma in hepatitis C cirrhosis through GC/MS and UPLC/MS-MS. Liver Intl. 2014; 34:1428–1444.
17. Zeng J, Yin P, Tan Y, et al. Metabolomics study of hepatocellular carcinoma: discovery and validation of serum potential biomarkers by using capillary electrophoresis-mass spectrometry. J Proteome Res. 2014; 13:3420–3431. [PubMed: 24853826]
18. Fages A, Duarte-Salles T, Stepien M, et al. Metabolomic profiles of hepatocellular carcinoma in a European prospective cohort. BMC Med. 2015; 13:242. [PubMed: 26399231]
19. Gao R, Cheng J, Fan C, et al. Serum metabolomics to identify the liver disease-specific biomarkers for the progression of hepatitis to hepatocellular carcinoma. Sci Rep. 2015; 5:18175. [PubMed: 26658617]
20. Huang Q, Tan Y, Yin P, et al. Metabolic characterization of hepatocellular carcinoma using nontargeted tissue metabolomics. Cancer Res. 2013; 73:4992–5002. [PubMed: 23824744]
21. Lewerenz J, Hewett SJ, Huang Y, et al. The cystine/glutamate antiporter system x(c)(−) in health and disease: from molecular mechanisms to novel therapeutic opportunities. Antioxid Redox Signal. 2013; 18:522–555. [PubMed: 22667998]
22. Baek S, Choi CM, Ahn SH, et al. Exploratory clinical trial of (4S)-4-(3-[18F]fluoropropyl)-L-glutamate for imaging xC- transporter using positron emission tomography in patients with non-small cell lung or breast cancer. Clin Cancer Res. 2012; 18:5427–5437. [PubMed: 22893629]

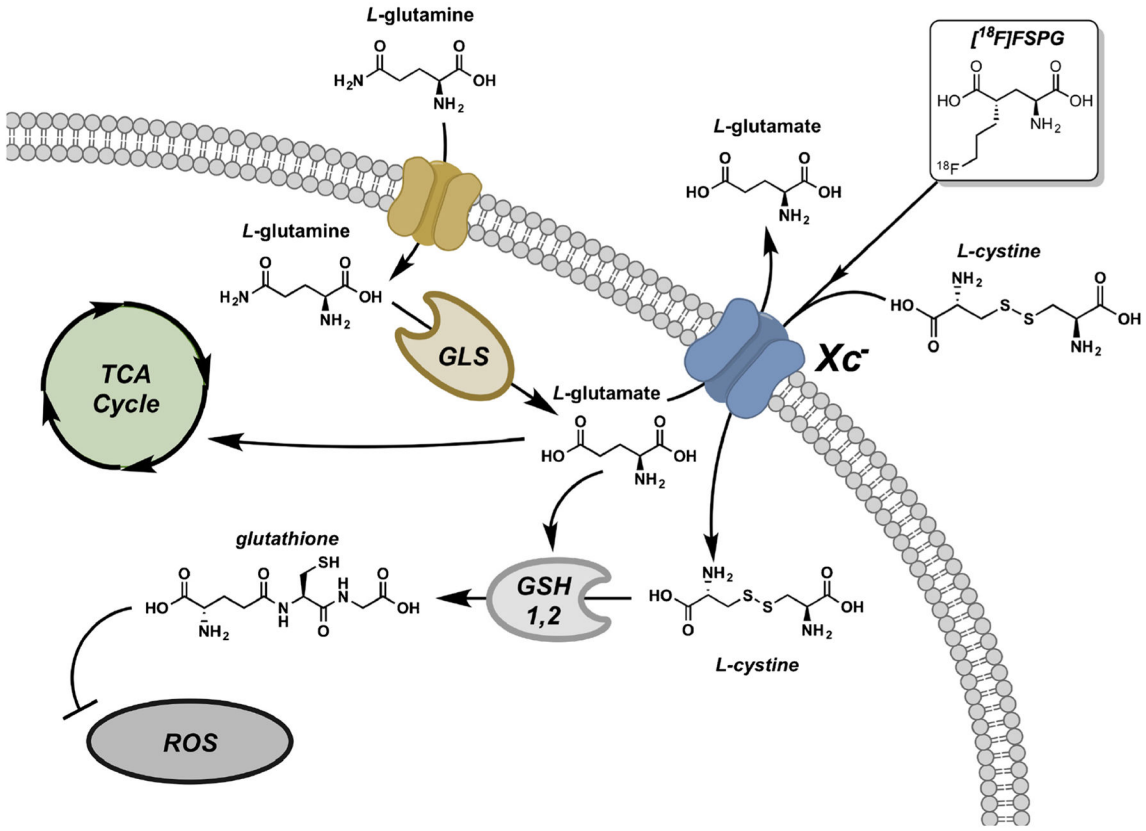

Fig. 1.

Truncated TCA cycle and [^{18}F]FSPG accumulation in cancer cells. As part of the truncated TCA cycle, L-glutamine is taken up via the ASCT2 transporter. L-glutamine is subsequently processed by GLS into L-glutamate, which is then used by the TCA cycle or transported out of the cell by the system x_{C-} transporter in exchange for L-cystine in a rate-limiting fashion. [^{18}F]FSPG biologically functions as L-cystine and is internalized by the system x_{C-} transporter. This provides precursors for glutathione biosynthesis and, thus, redox maintenance. *GLS* glutaminase, *GSH1* gamma-glutamyl cysteine synthetase, *GSH2* glutathione synthase, *ROS* reactive oxygen species.

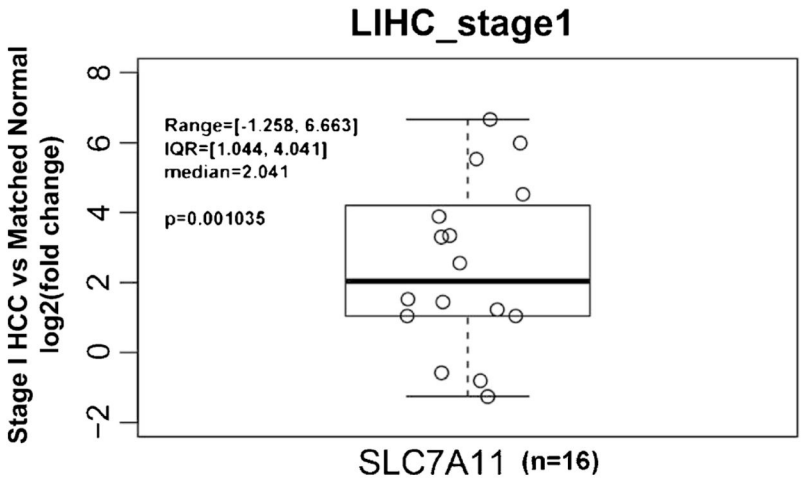

Fig. 2.

TCGA RNA-Seq analysis of *SLC7A11* expression in stage 1 HCC compared to matched non-tumor liver. Over 80 % of stage 1 HCCs exhibited *SLC7A11* expression that exceeded background liver in matched specimens ($n = 16$, $p < 0.01$) with more than 2-fold change.

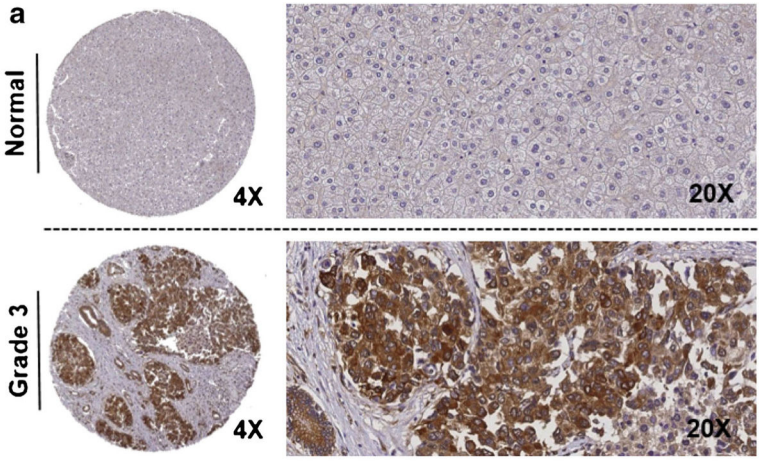

b

IHC Score	Population Frequency (%)		
	Grade 1, 2 (n = 27)	Grade 3, 4 (n = 56)	Total (n = 83)
Negative	48	19	29
Positive	52	81	71

Fig. 3.

Tumor microarray analysis of SLC7A11 expression levels by immunohistochemistry. **a** Typical level of staining for non-tumor liver, showing minimal immunoreactivity. In contrast, grade 3 HCC exhibits robust staining, with SLC7A11 immunoreactivity confined to tumor cells. Transporter localization localizes to the membrane, as expected. Magnifications (×4 and ×20) shown. **b** Statistical analysis of 83 tissue specimens from the Vanderbilt HCC cohort ($p = 0.006$).

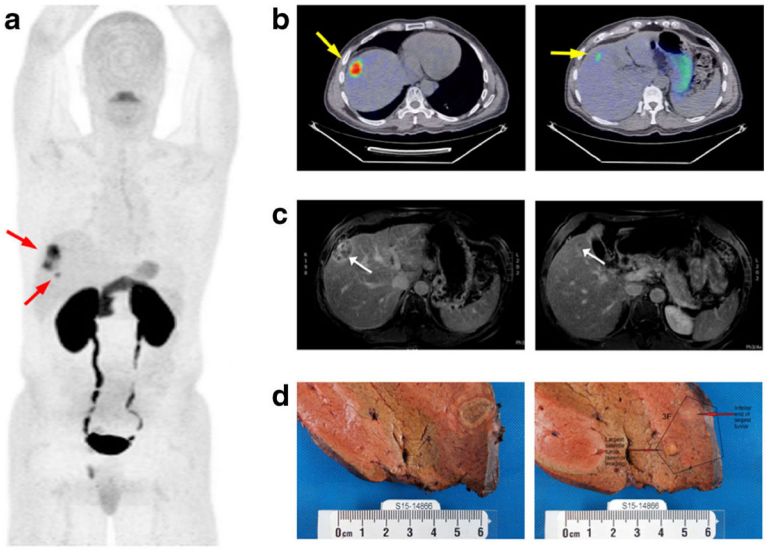

Fig. 4.

[^{18}F]FSPG PET images from a 62-year-old male diagnosed with HCC (patient 5). **a** 2D coronal maximum intensity projection (MIP) of skull to mid-thigh [^{18}F]FSPG PET scan showing two discrete areas of focal [^{18}F]FSPG avidity (*arrows*). **b** Axial [^{18}F]FSPG PET/CT fusion images corresponding to the two regions of uptake; PET images scaled to SUV 0–10 for comparison. **c** Delayed phase contrast-enhanced MRI of the main lesion (*left*) and satellite lesion (*right*). **d** Explanted pathological sections showing main lesion (*left*) and satellite lesion (*right*).

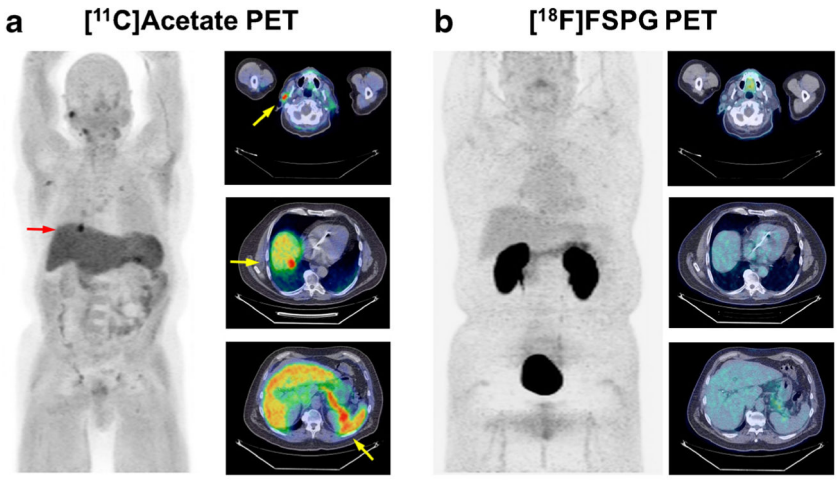

Fig. 5.

[^{11}C]acetate PET and [^{18}F]FSPG PET images from a 68-year-old male diagnosed with HCC (patient 2). Panels **a** and **b** show 2D coronal maximum intensity projections and axial PET/CT fusion (*inset*) images; PET images scaled to SUV 0–10 for comparison. Approximately 20 min following injection (7.9 MBq/kg/IV), focal [^{11}C]acetate accumulation was observed in the hepatic region (*arrow*), which did not show appreciable uptake of [^{18}F]FSPG relative to surrounding tissue 60 min following injection (2.5 MBq/kg/IV).

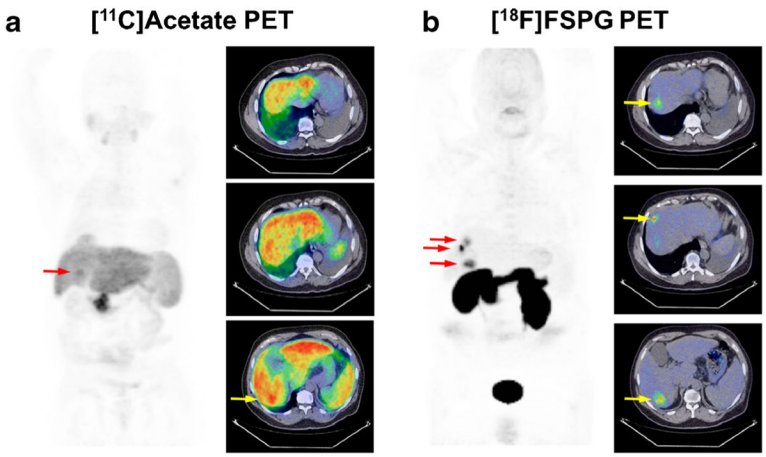

Fig. 6.

[^{11}C]acetate PET and [^{18}F]FSPG PET images from a 62-year-old male diagnosed with HCC (patient 10). Panels **a** and **b** show 2D coronal maximum intensity projections and axial PET/CT fusion images (*insets*); PET images scaled to SUV 0–10 for comparison. Approximately 20 min following [^{11}C]acetate (7.7 MBq/kg/IV), diffuse uptake and poor lesion contrast were observed. Conversely, 60 min following [^{18}F]FSPG PET (2.8 MBq/kg/IV), uptake was appreciably more focal and allowed clear delineation of three discrete areas of uptake within liver tissue (*arrows*).

Table 1

Patient demographics and [^{18}F]FSPG and [^{11}C]acetate PET imaging results

Pt no.	Age (y)	Sex	Tumor size (cm)	Cirrhosis	Other condition	[^{18}F]FSPG tumor (SUV_{MAX})	[^{18}F]FSPG liver (SUV_{MAX})	[^{18}F]FSPG tumor to liver	[^{18}F]FSPG detection	[^{11}C]acetate tumor (SUV_{MAX})	[^{11}C]acetate liver (SUV_{MAX})	[^{11}C]acetate tumor to liver	[^{11}C]acetate detection
1	52	M	2.6	Y	HCV; MD	2.5	1.0	2.5	Y	4.3	3.2	1.3	Y
2	68	M	2.8	Y	NASH; Hem	1.9	1.9	1.0	N	8.8	4.4	2.0	Y
3	38	M	4.0, 2.0	N	HCV	4.6, 2.4	1.7	2.7, 1.4	Y, Y	8.4, 6.4	6.1	1.4, 1.0	Y, Y
4	64	M	3.4	Y	HCV	1.9	1.0	1.9	Y	7.7	4.5	1.7	Y
5[a]	62	M	4.7, 1.2	N	HCV	9.2, 3.8	0.7	13.1, 5.4	Y, Y	–	–	–	–
6[b]	57	F	1.7	Y	–	0.7	0.5	1.4	Y	–	–	–	–
7[a]	66	M	3.0	N	HCV	1.1	0.7	1.6	Y	5.0	4.5	1.1	N
8	58	M	3.2	Y	HCV	0.6	0.9	0.7	N	–	–	–	–
9	77	M	2.1, 2.1	Y	–	1.0, 1.1	1.2	0.8, 0.9	N, N	–	–	–	–
10[b]	62	M	3.0, 4.0, 4.3	Y	HCV	6.0, 3.9, 5.4	1.2	5.0, 3.3, 4.5	Y, Y, Y	NS, NS, 7	4.9	NS, NS, 1.4	N, N, Y
11[a]	72	M	5.1	N	–	5.1	1.8	2.8	Y	7.6	4.0	1.9	Y

All patients scanned with [^{18}F]FSPG = 12/16 tumors detected for a detection rate of 75 %. For patients scanned with both [^{18}F]FSPG and [^{11}C]acetate, 9/10 tumors were detected by [^{18}F]FSPG for a detection rate of 90 % and 7/10 tumors were detected by [^{11}C]acetate for a detection rate of 70 %

Pt no. patient number, *y* years, *SUV* standardized uptake value, *HCV* hepatitis C, *PMD* porphyrin metabolism disorder, *NASH* non-alcoholic steatohepatitis, *Hem* hemochromatosis, *NS* not significant

[a] Moderately differentiated HCC

[b] Well-differentiated HCC